Journal of Nuclear Medicine, published on October 12, 2017 as doi:10.2967/jnumed.117.199596

Synthesis and biological evaluation of a novel ^{18}F-labeled Adnectin as a PET Radioligand for Imaging PD-L1 expression

David J. Donnelly[*†], R. Adam Smith[*], Paul Morin[*], Daša Lipovšek, Jochem Gokemeijer, Daniel Cohen, Virginie Lafont, Tritin Tran, Erin L. Cole, Martin Wright, Joonyoung Kim, Adrienne Pena, Daniel Kukral, Douglas D. Dischino, Patrick Chow, Jinping Gan, Olufemi Adelakun, Xi-Tao Wang, Kai Cao, David Leung, Samuel J. Bonacorsi Jr. and Wendy Hayes

Bristol-Myers Squibb Pharmaceutical Research and Development, P.O. Box 4000, Princeton, NJ 08543, USA.

[†]**Corresponding author:** David J. Donnelly, Ph.D.
Discovery Chemical Platforms-PET Radiochemical Synthesis, Bristol-Myers Squibb Pharmaceutical Research and Development, P.O. Box 4000, Princeton, NJ 08543, USA.
Telephone: 609-252-3884; Fax: 609-252-3307; E-mail: david.donnelly@bms.com

***Contributed equally to this work.**

Disclosure: All Authors in this manuscript are employed by Bristol-Myers Squibb Co. ^{18}F-BMS-986192 and ^{18}F-BMT-187144 are the subject of patent applications WO2016086021A1 and WO2016086036A2. No other potential conflict of interest relevant to this article was reported.

Word Count: Abstract: 346; Article: 4815

Running title: ^{18}F-labeled anti-PD-L1 Adnectin.

ABSTRACT

The programmed death protein (PD-1) and its ligand (PD-L1) play critical roles in a checkpoint pathway cancer cells exploit to evade the immune system. A same-day PET imaging agent for measuring PD-L1 status in primary and metastatic lesions could be important for optimizing drug therapy. Herein, we have evaluated the tumor targeting of an anti-PD-L1 Adnectin after ^{18}F-fluorine labeling.

Methods: An anti-PD-L1 Adnectin was labeled with ^{18}F in two steps. This synthesis featured fluorination of a novel prosthetic group, followed by a copper-free click conjugation to a modified Adnectin to generate ^{18}F-BMS-986192. ^{18}F-BMS-986192 was evaluated in tumors using *in vitro* autoradiography and PET using mice bearing bilateral PD-L1(-) and PD-L1(+) subcutaneous tumors. ^{18}F-BMS-986192 was evaluated for distribution, binding and radiation dosimetry in healthy cynomolgus monkey.

Results: ^{18}F-BMS-986192 bound to human and cynomolgus PD-L1 with a K_D of <35 pM, as measured by surface plasmon resonance (SPR). This Adnectin was labeled with ^{18}F to yield a PET radioligand for assessing PD-L1 expression *in vivo*. ^{18}F-BMS-986192 bound to tumor tissues as a function of PD-L1 expression determined by immunohistochemistry. Radioligand binding was blocked in a dose-dependent manner. *In vivo* PET imaging clearly visualized PD-L1 expression in mice implanted with a PD-L1(+), L2987 xenograft tumors. Two hrs after dosing, a 3.5-fold higher uptake (2.41 ± 0.29 vs. 0.82 ± 0.11 %ID/g, $p < 0.0001$) was observed in L2987 compared to control HT-29 (PD-L1(-)) tumors. Co-administration of 3 mg/kg ADX_5322_A02 anti-PD-L1 Adnectin reduced tumor uptake at 2 hrs post-injection by approximately 70%, while HT-29 uptake remained unchanged,

demonstrating PD-L1 specific binding. Biodistribution in non-human primate showed binding in the PD-L1 rich spleen with rapid blood clearance through the kidneys and bladder. Binding in the PD-L1(+) spleen was reduced by co-administration of BMS-986192. Dosimetry estimates indicate that the kidney is the dose-limiting organ with an estimated human absorbed dose of 2.20E-01 mSv/MBq.

Conclusion: ^{18}F-BMS-986192 demonstrated the feasibility of non-invasively imaging the PD-L1 status of tumors by micro-PET studies. Clinical studies with ^{18}F-BMS-986192 are underway to measure PD-L1 expression in human tumors.

Keywords: PD-L1, PET, PD-1/PD-L1 checkpoint inhibitor, ^{18}F-labeled Adnectin, ^{18}F-BMS-986192

INTRODUCTION

A healthy immune system maintains a delicate balance between eradicating infections/cancers and maintaining self-tolerance. The immune system accomplishes this in part by the expression of immune checkpoints that control immune response. However, tumors exploit these checkpoint pathways by expressing co-inhibitory proteins to evade anti-tumor immune responses (*1*). One major checkpoint inhibitor pathway is the PD-1 pathway. PD-1 is a negative costimulatory receptor expressed on the surface of activated T and B-cells (*2,3*). PD-L1 is a surface glycoprotein ligand for PD-1 that facilitates immunosuppression on both antigen-presenting cells and human cancers. PD-L1 downregulates T-cell activation and cytokine secretion by binding to PD-1 (*4,5*). Several antibodies directed against the PD-1/PD-L1 pathway have been developed to treat a wide variety of cancers (*6-10*). Elevated PD-L1 expression is correlated with poor prognosis in some cancers, which suggests that PD-L1 upregulation is a mechanism for tumor immune evasion (*11*). The predictive role of PD-L1 expression on tumor cells has been an active area of research and several immunohistochemistry assays have been developed to predict responses to either anti-PD-1 or anti-PD-L1 treatment (*12*). However, these measures are limited as typically only a single patient biopsy sample is evaluated for PD-L1 expression using immunohistochemistry (*13,14*). A PD-L1 PET radioligand represents a noninvasive tool that is complementary to immunohistochemistry, which allows for serial imaging of PD-L1 expression in both primary and metastatic tumors. In addition, this tool could measure *in vivo* dynamic changes in PD-L1 expression during, and after treatment with immune checkpoint modulating drugs without needle biopsy (*15*).

Recently, there has been a resurgence in the application of antibody based imaging agents and several imaging agents targeting PD-L1 have recently been reported in the literature using this framework (*16–21*). These agents offer the affinity and specificity needed to maximize signal to background ratios for visualizing a molecular target within the tumor microenvironment. However, one disadvantage of antibody based imaging agents is their slow clearance. Typically, antibodies are cleared through the hepatobiliary system over a period of days to weeks, making imaging in neighboring organs such as the lung a challenge. As a result, it can take many days for these agents to sufficiently clear target free tissues or neighboring tissues to enable imaging. An ideal PD-L1 PET radioligand is one that offers high tumor uptake in PD-L1 positive tumors, low background signal in non-PD-L1 expressing tissues and enables same day imaging for patients for flexibility in clinical study design (*22*).

Adnectins are a family of engineered, target binding proteins that are derived from the 10^{th} type III domain of human fibronectin (10Fn3). The 10Fn3 structure resembles antibody variable domains, having two sets of antiparallel beta sheets with solvent accessible loops at each pole (*23,24*). These loops can be engineered to provide high binding affinity to a wide variety of targets. Adnectins have several advantages as targeting domains for molecular imaging agents. Their smaller size (~10 kDa), allows for good image contrast with rapid delivery to targeted tissues and fast glomerular clearance of unbound probe to drive image contrast. Adnectins have high stability and the absence of cysteine or disulfide bonds allows the introduction of a single cysteine for site specific conjugation of PET radionuclides. Herein is presented the preliminary evaluation of a

fluorine-18 labeled Adnectin as a same day *in vivo* PET radioligand to quantify PD-L1 expression in tumors.

MATERIALS AND METHODS

Adnectin production and conjugation of DBCO with ADX_5322_A02, SPR, immunohistochemistry, fluorescence-activated cell sorting, cell lines and radiation dosimetry are found in the Supplementary Methods section.

Synthesis of ^{18}F-BMS-986192

^{18}F-fluoride (29.6 GBq) was transferred through a pre-conditioned anion exchange cartridge and eluted with potassium carbonate (3 mg) and 4,7,13,16,21,24-hexaoxa-1,10-diazabicyclo[8.8.8]hexacosane (15 mg) in 1.4 mL of acetonitrile. The solvent was azeotroprically dried and to this mixture was added (3-(2-(2-(2-(2-azidoethoxy)ethoxy)ethoxy)ethoxy)-2-nitropyridine (2 mg) in 0.5 mL of DMSO. This solution was heated at 120 °C for 10 mins, followed by dilution with 3 mL of water and transferred onto a Luna C18 (250 x 10 mm) HPLC column. The prosthetic group, ^{18}F-BMT-187144 was purified using a mobile phase mixture of 32% acetonitrile in 0.1% trifluoroacetic acid at a flow rate of 4.6 mL/min. ^{18}F-BMT-187144 was collected into a 100 mL flask that contained 25 mL of water and its contents were delivered to a C18 cartridge. ^{18}F-BMT-187144 was released from the cartridge with 3 mL of ethanol, evaporated to dryness and reconstituted into 0.1 mL of sterile water. To this solution was added 0.2 mL of ADX_5322_A02-DBCO (3 mg/mL) in phosphate buffered saline (PBS). The reaction mixture was gently mixed for 45 mins at 45 °C. ^{18}F-BMS-986192 was purified using a Superdex 200 10/300 GL size exclusion column and 1X PBS mobile phase at 0.5 mL/min flow rate. ^{18}F-BMS-986192 was isolated over a 5 min period and passed through a 0.2

micron polyethersulfone membrane filter and into a sterile vial as the final formulated product. The radiochemical purity was determined using an HPLC (Agilent) system and a Posi-Ram (INUS) radio-HPLC detector. Methods for quality control and specific activity of ^{18}F-BMS-986192 are found in the Supplementary Methods section and Supplemental Figures 1-3.

Animal Models

All procedures involving animal studies were reviewed and approved by the Bristol-Myers Squibb animal care and use committee. *In vivo* studies were performed by implanting tumor xenografts in 5-6 week old female athymic nude mice (Charles River). The L2987 is a human lung carcinoma cell line and the HT-29 is a colon adenocarcinoma carcinoma cell line (American type culture collection). Bilateral tumor xenografts were established by subcutaneous inoculation of HT-29 (1.5E06 cells) and L2987 (4E06 cells) in contralateral shoulders in a total injection volume of 0.2 mL. Once tumors reached approximately 300 mm^3 animals were selected for imaging.

Autoradiography

HT-29/L2987 tumors were excised two weeks from the implantation date. Replicate sets of 5 μm thick cryosections were prepared and adhered to glass slides. 5 μm fresh frozen human non-small cell lung cancer (NSCLC) tumor samples were also obtained (Asterand). Slides were pre-incubated for 20 mins using a protein block solution (Dako), then transferred to glass incubation chambers that contained 40 mL buffer (1X PBS supplemented with 0.5% bovine serum albumin) and 0.25 nM solution of ^{18}F-BMS-986192. Several samples were co-incubated with BMS-986192 at 0.025, 0.25, 2.5, and 25 nM or a non-PD-L1 binding (sham) Adnectin (25 nM). These slides were incubated for 1

hr at room temperature and then were washed 4 times with ice-cold buffer for 3 mins. Slides were air dried at room temperature and affixed to a phosphorimaging plate (BAS-SR 3545S) and exposed for 15 mins. Plates were scanned using a bioimaging analyzer (Fujifilm, FLA-9000). Image analysis was performed using multi-gauge software.

Small Animal PET Imaging

Mice were anesthetized with isoflurane in oxygen (2% induction and maintenance), tail vein catheters were installed then transferred to the microPET F120 scanner (Siemens). A 10-min transmission image was acquired using a ^{57}Co point source for attenuation correction of the final PET images. Then ~5.6 MBq ^{18}F-BMS-986192 (n = 7) was administered via the tail vein. Two hr dynamic emission images were acquired for all animals. For blocking studies, animals (n = 4) received 3 mg/kg ADX_5322_A02 anti-PD-L1 Adnectin co-administered with ^{18}F-BMS-986192. PET data was reconstructed using a 3D ordered-subsets expectation maximization followed by maximum a posteriori algorithm corrected for attenuation using the previously acquired transmission scan. Image analysis was performed using ASIPro software (Siemens) with regions of interest drawn around tumors and radiotracer uptake expressed as percent injected dose per gram (%ID/g).

***Ex Vivo* Biodistribution**

^{18}F-BMS-986192 was also co-administered for ex vivo biodistribution studies with varying concentrations of BMS-986192 in a single syringe to alter the effective specific activity of the administered tracer dose. Animals in each group (n = 4) received ~5.6 MBq ^{18}F-BMS-986192 with effective specific activities of 14.1 MBq/nmol, 7.1 MBq/nmol, 2.8 MBq/nmol, 1.4 MBq/nmol, or 0.7 MBq/nmol. 90 minutes after injection, the mice were euthanized and the blood, liver, kidneys, spleen, heart, lung, stomach, muscle, bone, HT-

29 and L2987 tumors were collected and measured using a gamma counter (Perkin-Elmer, Wallac3).

Cynomolgus PET Imaging

Animals were anesthetized with an intramuscular injection of 0.02 mg/kg Atropine, 5 mg/kg Telazol, and 0.01 mg/kg Buprenorphine. Catheters were placed into the saphenous and cephalic veins and animals were intubated and transferred to the microPET F220 (Siemens). Anesthesia was maintained with isoflurane and oxygen. I.V. fluids (lactated ringers solution) were administered throughout the scan. Transmission images using a ^{57}Co point source were acquired over 5 individual bed positions (10 mins per position) to image from the top of head to lower leg of the animal. Adjacent bed positions were set to overlap by 1.5 cm. ~55.5 MBq ^{18}F-BMS-986192 was administered via the saphenous catheter. Emission images were acquired in a sequence of 5 passes over the previous 5 bed positions (5 min per position), producing a series of "whole body" images covering a duration of ~150 min post-tracer administration. Images were reconstructed using a filtered back projection algorithm with attenuation correction using the ^{57}Co transmission scans, and corrected for decay. A blocking study in the same non-human primate was conducted 24 hrs after the first baseline imaging study. This study followed the procedure described above only tracer was co-administered with 1 mg/kg BMS-986192.

RESULTS

Selection and Radiolabeling of Anti-PD-L1 Adnectin

An anti-PD-L1 Adnectin (ADX_5322_A02) was selected *in vitro,* produced, characterized and successfully labeled with fluroine-18. SPR analysis was utilized to

determine the kinetic parameters of ADX_5322_A02 and BMS-986192 as it bound to human or cynomolgus PD-L1 (Supplemental Fig.4). BMS-986192 shows no appreciable difference in binding parameters to its unmodified counterpart ADX_5322_A02 (Supplemental Table 1). This Adnectin displayed picomolar dissociation constants (K_D < 35 pM) against both human and cynomolgus PD-L1 (near the limit of detection via SPR) and did not bind to murine PD-L1 (Supplemental Table 2).

A fluorine-18 labeled derivative of ADX_5322_A02 anti-PD-L1 Adnectin was synthesized utilizing a fluorine-18 prosthetic group, ^{18}F-BMT-187144 (Fig. 1). ^{18}F-BMT-187144 was generated in high radiochemical yield (>70% non-decay corrected yield, *n* = 40), in >90% radiochemical purity, was stable in a PBS solution over 1 hr and was reduced to dryness without loss of radioactivity enabling efficient protein labeling with fluorine-18 (Supplemental Methods). The ^{18}F-BMT-187144 prosthetic group was then used to synthesize ^{18}F-BMS-986192 as shown in Figure 2, using copper-free "click" chemistry. 1.1 ± 0.3 GBq (*n* = 15) of ^{18}F-BMS-986192 was isolated, starting from 29.6 GBq of ^{18}F-fluoride with 96 ± 3% radiochemical purity and a specific activity of 63 ± 3 MBq/nmol.

Characterization of PD-L1 Expression in HT-29 and L2987 Xenografts

HT-29 and L2987 xenograft tumor models were investigated with regard to PD-L1 expression using fluorescence-activated cell sorting, immunohistochemistry, autoradiography and *in vivo* biodistribution in an immunocompromised mouse model. Fluorescence-activated cell sorting of these cells and immunohistochemistry analysis of xenograft tissues derived from these cell lines show moderate expression of PD-L1 in the L2987 model while HT-29 was confirmed as a negative control with little/no PD-L1 expression (Figs. 3A and 3B). Autoradiography of these xenograft tissues showed

increased ^{18}F-BMS-986192 binding to L2987 (14.0 ± 1.0 PSL/mm^2) compared to control HT-29 (1.59 ± 0.5 PSL/mm^2) (Fig. 3C).

Autoradiography in Human NSCLC Tissue Samples

^{18}F-BMS-986192 binding was assessed in a panel of 6 human NSCLC samples (Fig. 3C). ^{18}F-BMS-986192 exhibited increased total radioligand binding in all of the tested human tissues compared to the xenograft tissues, ranging from 21.35 - 230.79 PSL/mm^2 (Table 1). Specificity of binding to tissue samples was evaluated in blocking studies by co-incubation with excess BMS-986192. Dose-dependent blockade of ^{18}F-BMS-986192 binding to all PD-L1 positive tissues was seen with increasing concentration of blocking agent (Fig. 3C; Table 1). At 25 nM concentration of BMS-986192, radiotracer binding was reduced by 75 - 95% in the human NSCLC tissue samples. Co-incubation with 25 nM of a non-PD-L1 binding "sham" Adnectin resulted in no appreciable change in radiotracer binding to any tissue sample, confirming the specificity of ^{18}F-BMS-986192 binding. ^{18}F-BMS-986192 binding demonstrated concordance with PD-L1 immunohistochemistry staining (Fig. 3B and 3C) in human NSCLC tissues.

Small Animal PET Imaging and Biodistribution

To evaluate the potential of ^{18}F-BMS-986192 as a PET radioligand for PD-L1, PET imaging in xenograft models was performed. Representative PET whole body coronal images of mice with bilateral HT-29 and L2987 xenografts demonstrated increased accumulation of ^{18}F-BMS-986192 in the moderate PD-L1 expressing L2987 compared to control HT-29 tumors with negligible PD-L1 expression (2.41 ± 0.29 vs. 0.82 ± 0.11 %ID/g, $p < 0.0001$; Fig. 4A). Tracer uptake in peripheral organs (e.g. liver, lung, heart, etc.) was moderate and uptake in muscle was minimal, resulting in high-contrast images.

Tracer accumulation in L2987 tumors plateaued between 90-120 min post tracer administration (Fig. 4B).

Specificity of ^{18}F-BMS-986192 binding was further confirmed in blocking studies in which excess BMS-986192 was co-injected along with the radiotracer. Accumulation of ^{18}F-BMS-986192 in L2987 tumors was reduced by 70% compared to mice that received the radiotracer alone (Fig. 4A). Resulting uptake in PD-L1(+) L2987 tumors was similar to the PD-L1(-) HT-29 tumor (0.79 ± 0.12 vs. 0.71 ± 0.15 %ID/g, $p = 0.44$), demonstrating near complete blockade of specific tracer uptake and suggesting that tumor accumulation of ^{18}F-BMS-986192 in the L2987 xenograft model was consistent with specific binding. *Ex vivo* biodistribution studies confirmed significantly higher uptake in L2987 compared to control HT-29 tumors and to other peripheral tissues (Fig. 5A). Tracer uptake was 3.5-4 fold higher than in PD-L1(-) HT-29 control tumors. The only tissue with higher uptake was the kidney, which is consistent with its role in clearance. The ratio of tracer uptake in L2987 tumors to various background tissues (HT-29 tumor, muscle, and blood) was measured following co-administration of increasing doses of BMS-986192 (Fig. 5B). These studies indicated a dose-dependent blockade of radiotracer accumulation in L2987 tumors, resulting in a reduced uptake ratio. The highest blocking dose (tracer specific activity of 0.7 MBq/nmol) showed a complete elimination of tumor contrast, confirming the specific nature of ^{18}F-BMS-986192 binding *in vivo*.

Cynomolgus Imaging

PET imaging in a healthy cynomolgus monkey using ^{18}F-BMS-986192 showed an accumulation of tracer in the PD-L1(+) spleen tissue, reaching a 12:1 ratio compared to muscle. Overall background signal was low, with little accumulation outside of the spleen

and clearance organs of kidney and urinary bladder (Fig. 6A). Accumulation in the PD-L1(+) spleen was reduced approximately 90% to near background levels with co-administration of 1 mg/kg BMS-986192 (Fig. 6B), reducing the spleen:muscle ratio to (1.24:1). The reduction of specific radiotracer accumulation in the spleen is consistent with moderate PD-L1 staining seen by immunohistochemistry (Fig. 6C).

Dosimetry results indicate that the distribution of ^{18}F-BMS-986192 is similar between male and female animals. The kidney is the dose-limiting organ with an estimated absorbed dose for the average human subject of 2.20E-01 mSv/MBq (Supplemental Table 3). Under RDRC exposure limits as specified in 21 CFR 361.1, this yields an estimated single study administration dose of 228 MBq for the average human subject.

Discussion

The goal of this work was to develop an ^{18}F-labeled radioligand to enable non-invasive, same day imaging of PD-L1 expression in living tissues. This tool allows for a longitudinal measurement of PD-L1 expression within the tumor microenvironment prior to, during and following therapeutic intervention. Recently, several PD-L1 imaging agents have demonstrated feasibility of evaluating PD-L1 expression (*16,19,20,25,26*).

Adnectins are an attractive scaffold for same day PET imaging of this target as they demonstrate high target affinity and rapid tumor uptake. Similar to peptide based scaffolds, Adnectins also have rapid clearance from blood and background tissues (*26–29*). A recent study with an EGFR binding Adnectin labeled with a PET radionuclide showed the feasibility of using this scaffold to generate a tracer targeting EGFR receptors in tumors with high signal to noise ratios (*28*).

^{18}F is an attractive radionuclide for labeling Adnectins given its: 97% emission via positron emission, high theoretical specific activity of 63 TBq/μmol, and 109.5 min half-life, which matches the <2 hr blood half-life of Adnectins in humans (*23,30*). To incorporate ^{18}F labeling, the Adnectin was engineered with a cysteine residue on the c-terminus of the protein, on the opposite pole of the variable loops assumed to confer PD-L1 binding. This placement allowed the PET labeling motifs to be attached distal from the PD-L1 recognition residues. SPR data confirmed that these modifications did not have an effect on the binding of this Adnectin, which remained in the picomolar range. The strategy for ^{18}F labeling was to conjugate the anti-PD-L1 Adnectin with a ^{18}F prosthetic group using copper-free "click" chemistry and a commercially available ring-constrained DBCO-PEG4-maleimide moiety. This bio-orthogonal agent enabled site specific modification at the engineered cysteine residue without compromising the stability or affinity of the Adnectin protein.

Efforts were made to use previously described prosthetic groups to label the Adnectin platform with fluorine-18, including the azide containing 1-azido-2-(2-(2-(2-fluoroethoxy)ethoxy)ethoxy)ethane (*31*). Unfortunately, this approach did not yield the desired product. Under dilute reaction conditions needed to keep the total volume of ethanol in the reaction solution below 10% (for Adnectin stability) no ^{18}F-labeling occurred. Attempts to concentrate the crude reaction solution led to ethanol concentrations above 10%, which led to aggregation of the Adnectin. Further attempts to concentrate this prosthetic group in solution volatilized the product. To solve this issue, a nitropyridine was incorporated (Fig. 1) which allowed for rapid ^{18}F incorporation into the molecule and provided a non-volatile prosthetic group. This allowed for the complete removal of organic

solvents with minimal radioactivity loss (Supplemental, Table 4). The product could then be reconstituted in aqueous buffer for stability of the Adnectin. The novel labeled prosthetic group was stable in this buffer system for over an hour (Supplemental, Fig. 5) and enabled efficient ^{18}F labeling of the PD-L1 Adnectins.

^{18}F-BMS-986192 shows PD-L1 specific uptake in tumor tissues. *In vitro* autoradiography experiments demonstrated higher binding to PD-L1(+) compared to PD-L1(-) xenograft tissues in a 9:1 ratio. Studies with human NSCLC tissues demonstrated similar results (Fig. 3C). ^{18}F-BMS-986192 binding in human NSCLC tissues was proportional to PD-L1 staining by immunohistochemistry (Figs. 3B and 3C). Co-administration with BMS-986192 reduced radioligand binding in both the human NSCLC and L2987 xenograft tissues by >80%, with minimal effect observed in PD-L1(-) tissues. Finally, radioligand binding of ^{18}F-BMS-986192 was not affected by co-administration of a non-PD-L1 binding "sham" Adnectin (Fig. 3C). These results suggest ^{18}F-BMS-986192 retains its high affinity and specificity to the PD-L1 receptor.

PET imaging with this tracer in mice implanted with both PD-L1(+) and PD-L1(-) xenografts demonstrated rapid accumulation in the PD-L1(+) tumor and minimal signal in the PD-L1(-) tumor (Fig. 4). Using ^{18}F-BMS-986192, the PD-L1(+) xenograft was visualized in 3.6:1 ratio over the PD-L1(-) tumor *in vivo* and the tumor to muscle ratio remained high (>11:1) providing high contrast images (Fig. 4A). Co-injection of BMS-986192 reduced accumulation of the radioligand in PD-L1(+) tumors by >70% to a similar level as the PD-L1(-) tumor, confirming the specific nature of ^{18}F-BMS-986192 accumulation in L2987 xenografts (Fig. 4B and 4C). Collectively, the *in vitro* and *in vivo* results show that ^{18}F-BMS-986192 can be used to measure PD-L1 expression in tumors.

Since ^{18}F-BMS-986192 does not bind to mouse PD-L1, a study was performed to understand biodistribution in a model with endogenous PD-L1 expression. Picomolar dissociation constants were observed in non-human primate and immunohistochemistry showed moderate PD-L1 expression in the cynomolgus spleen (Fig. 6C). PET studies confirmed that background accumulation of ^{18}F-BMS-986192 was minimal, with little signal outside of the spleen, kidney, and urinary bladder (Fig. 6A). Accumulation in the PD-L1(+) spleen of the same non-human primate was reduced to background with co-administration of 1 mg/kg BMS-986192 (Fig. 6B). The reduction of radiotracer accumulation in the spleen is consistent with specific binding, since moderate PD-L1 staining was seen by immunohistochemistry (Fig. 6C).

The advantages of the ^{18}F-Adnectin platform described herein have been demonstrated through experiments with ^{18}F-BMS-986192. Time activity curves showed ^{18}F-BMS-986192 rapidly cleared through the kidney, with peak radioactivity observed at 25 min post injection in mice. Given the prolonged kidney retention observed with similar protein-based tracers using chelating agents or prolonged liver clearance seen with monoclonal antibody tracers coupled with the clinical utility of same day imaging, the advantages of ^{18}F-BMS-986192 as a PD-L1 radioligand are clear (*32*). No radioactive metabolites were seen with ^{18}F-BMS-986192 two hrs post-injection and pharmacokinetic studies show BMS-986192 is excreted as an intact molecule (Supplemental Figs. 6 and 7). From an imaging perspective, renal clearance of ^{18}F-BMS-986192 offers a distinct advantage over monoclonal antibody imaging agents for PD-L1 that are cleared through the liver depositing their radio-metal when catabolized, potentially masking tumors therein. The rapid blood clearance of ^{18}F-BMS-986192 provides an advantage compared to other

monoclonal antibody based PD-L1 immuno-PET agents such as ^{64}Cu/^{89}Zr-Atezolizumab that require imaging several days post injection of the tracer (*20*).

CONCLUSION

A novel ^{18}F-labeled Adnectin radioligand was developed for PET imaging of PD-L1 expressing tissues. In addition, an improved methodology was described based on a unique prosthetic group that allows for the ^{18}F labeling of Adnectins under mild conditions. Using copper-free "click" chemistry, ^{18}F-BMS-986192 was generated with picomolar affinity toward the human PD-L1 receptor in high radiochemical purity and high specific activity. This methodology addresses important issues associated with the ^{18}F labeling of proteins and should be applicable to related systems. *In vivo* imaging demonstrated rapid delivery of ^{18}F-BMS-986192 to PD-L1 expressing tumors and rapid clearance from non-PD-L1 expressing tumors and tissues. ^{18}F-BMS-986192 was highly stable *in vivo* and had low background signals in organs of interest such as the lung. The results of this study demonstrate the feasibility of preparing ^{18}F anti-PD-L1 Adnectins for the measurement of PD-L1 expression in tumors. Radiation dosimetry estimates indicate that this tracer is safe to administer in human studies. Clinical studies with ^{18}F-BMS-986192 are currently underway to better understand this checkpoint pathway and PD-L1 expression in human tumors.

DISCLOSURE

The costs of publication of this article were defrayed by the payment of page charges. Therefore, and solely to indicate this fact, this article is hereby marked "advertisement" in accordance with 18 USC section 1734. ^{18}F-BMS-986192 and ^{18}F-BMT-187144 are the subject of patent applications WO2016086021A1 and WO2016086036A2.

All authors were employees of Bristol-Myers Squibb Co. at the time of this work. No other potential conflict of interest relevant to this article was reported.

ACKNOWLEDGEMENTS

The authors would like to thank Amy Bertino, Alex Bush, Elliot Ethridge, David Fabrizio, Pallavi Gambhire, Ben Henley, Zheng Lin, David Linsenmayer, Sarah Maas, Frank Marsilio, Doug McLaughlin, Tracy Mitchell, John Newitt, Ted Pellas, Michael Pietras, Katie Russo and Kevin Smith for their efforts in support of the work generated in this manuscript.

REFERENCES

1. Pardoll DM. The blockade of immune checkpoints in cancer immunotherapy. *Nat Rev Cancer.* 2012;12:252-264.

2. Riella LV, Paterson AM, Sharpe AH, Chandraker A. Role of the PD-1 pathway in the immune response. *Am J Transplant.* 2012;12:2575-2587.

3. Keir ME, Butte MJ, Freeman GJ, Sharpe AH. PD-1 and its ligands in tolerance and immunity. *Annu Rev Immunol.* 2008;26:677-704.

4. Herbst RS, Soria JC, Kowanetz M, et al. Predictive correlates of response to the anti-PD-L1 antibody MPDL3280A in cancer patients. *Nature.* 2014;515:563-567.

5. Freeman GJ, Long AJ, Iwai Y, et al. Engagement of the PD-1 immunoinhibitory receptor by a novel B7 family member leads to negative regulation of lymphocyte activation. *J Exp Med.* 2000;192:1027-1034.

6. Kazandjian D, Suzman DL, Blumenthal G, et al. FDA approval summary: Nivolumab for the treatment of metastatic non-small cell lung cancer with progression on or after platinum-based chemotherapy. *Oncologist.* 2016;21:634-642.

7. Gyawali B, Ota A, Ando Y. Nivolumab in nonsquamous non-small-cell lung cancer. *N Engl J Med.* 2016;374:493.

8. Borghaei H, Brahmer J. Nivolumab in nonsquamous non-small-cell lung cancer. *N Engl J Med.* 2016;374:493-494.

9. Herbst RS, Baas P, Kim DW, et al. Pembrolizumab versus docetaxel for previously treated, PD-L1-positive, advanced non-small-cell lung cancer (KEYNOTE-010): a randomised controlled trial. *Lancet.* 2016;387:1540-1550.

10. Weinstock M, McDermott D. Targeting PD-1/PD-L1 in the treatment of metastatic renal cell carcinoma. *Ther Adv Urol.* 2015;7:365-377.

11. He J, Hu Y, Hu M, Li B. Development of PD-1/PD-L1 pathway in tumor immune microenvironment and treatment for non-small cell lung cancer. *Sci Rep.* 2015;5:13110.

12. Chakravarti N, Prieto VG. Predictive factors of activity of anti-programmed death-1/programmed death ligand-1 drugs: immunohistochemistry analysis. *Transl Lung Cancer Res.* 2015;4:743-751.

13. Topalian SL, Taube JM, Anders RA, Pardoll DM. Mechanism-driven biomarkers to guide immune checkpoint blockade in cancer therapy. *Nat Rev Cancer.* 2016;16:275-287.

14. Patel SP, Kurzrock R. PD-L1 Expression as a predictive biomarker in cancer immunotherapy. *Mol Cancer Ther*. 2015;14:847-856.

15. Ilie M, Long-Mira E, Lassalle S, et al. Comparative study of the PD-L1 status between surgically resected specimens and matched biopsies of NSCLC patients reveal major discordances: a potential issue for anti-PD-L1 therapeutic strategies. *Ann Oncol.* 2016;27:147-153.

16. Chatterjee S, Lesniak WG, Gabrielson M, et al. A humanized antibody for imaging immune checkpoint ligand PD-L1 expression in tumors. *Oncotarget.* 2016;7:10215-10227.

17. Wu AM. Antibodies and antimatter: the resurgence of immuno-PET. *J Nucl Med.* 2009;50:2-5.

18. Wu AM. Engineering Multivalent Antibody Fragments for *In Vivo* Targeting. In: Lo BKC, ed. *Antibody Engineering: Methods and Protocols*. Totowa, NJ: Humana Press; 2004:209-225.

19. Hettich M, Braun F, Bartholoma MD, Schirmbeck R, Niedermann G. High-Resolution PET Imaging with Therapeutic Antibody-based PD-1/PD-L1 Checkpoint Tracers. *Theranostics.* 2016;6:1629-1640.

20. Lesniak WG, Chatterjee S, Gabrielson M, et al. PD-L1 detection in tumors using ^{64}Cu-atezolizumab with PET. *Bioconjugate Chem.* 2016;27:2103-2110.

21. Heskamp S, Hobo W, Molkenboer-Kuenen JD, et al. Noninvasive imaging of tumor PD-L1 expression using radiolabeled anti-PD-L1 antibodies. *Cancer Res.* 2015;75:2928-36.

22. Olafsen T, Sirk SJ, Olma S, Shen CKF, Wu AM. ImmunoPET using engineered antibody fragments: fluorine-18 labeled diabodies for same-day imaging. *Tumor Biol.* 2012;33:669-677.

23. Lipovšek D. Adnectins: engineered target-binding protein therapeutics. *Protein Engineering Design and Selection.* 2011;24:3-9.

24. Koide A, Koide S. Monobodies: antibody mimics based on the scaffold of the fibronectin type III domain. *Methods Mol Biol.* 2007;352:95-109.

25. Maute RL, Gordon SR, Mayer AT, et al. Engineering high-affinity PD-1 variants for optimized immunotherapy and immuno-PET imaging. *Proc Natl Acad Sci U S A.* 2015;112:E6506-6514.

26. Chatterjee S, Lesniak WG, Miller MS, et al. Rapid PD-L1 detection in tumors with PET using a highly specific peptide. *Biochem Biophys Res Commun.* 2017;483:258-263.

27. Rossin R, Berndorff D, Friebe M, Dinkelborg LM, Welch MJ. Small-animal PET of tumor angiogenesis using a ^{76}Br-labeled human recombinant antibody fragment to the ED-B domain of fibronectin. *J Nucl Med.* 2007;48:1172-1179.

28. Hackel BJ, Kimura RH, Gambhir SS. Use of ^{64}Cu-labeled fibronectin domain with EGFR-overexpressing tumor xenograft: molecular imaging. *Radiology.* 2012;263:179-188.

29. Natarajan A, Hackel BJ, Gambhir SS. A novel engineered anti-CD20 tracer enables early time PET imaging in a humanized transgenic mouse model of B-cell non-Hodgkins lymphoma. *Clin Cancer Res.* 2013;19:6820-6829.

30. Weissleder R, Ross BD, Rehemtulla A, Gambhir SS. *Molecular Imaging, Principles and Practices* Vol 13: Peoples Medical Publishing House-USA; 2011.

31. Gill HS, Marik J. Preparation of ^{18}F-labeled peptides using the copper(I)-catalyzed azide-alkyne 1,3-dipolar cycloaddition. *Nat Protocols.* 2011;6:1718-1725.

32. Akizawa H, Uehara T, Arano Y. Renal uptake and metabolism of radiopharmaceuticals derived from peptides and proteins. *Advanced Drug Delivery Reviews*. 2008;60:1319-1328.

FIGURES

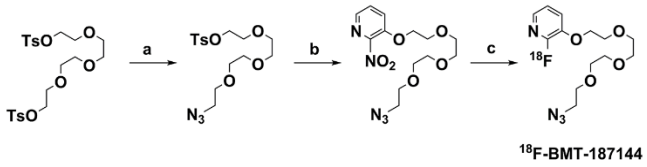

FIGURE 1. Synthesis of ^{18}F-BMT-187144. Reagents and Conditions: a) NaN_3, ethanol 90 °C 17 hrs; b) NaH, 2-nitropyridin-3-ol 0-60 ^{o}C, 4 hrs; c) K.2.2.2 K^{18}F, DMSO 120 °C 10 mins.

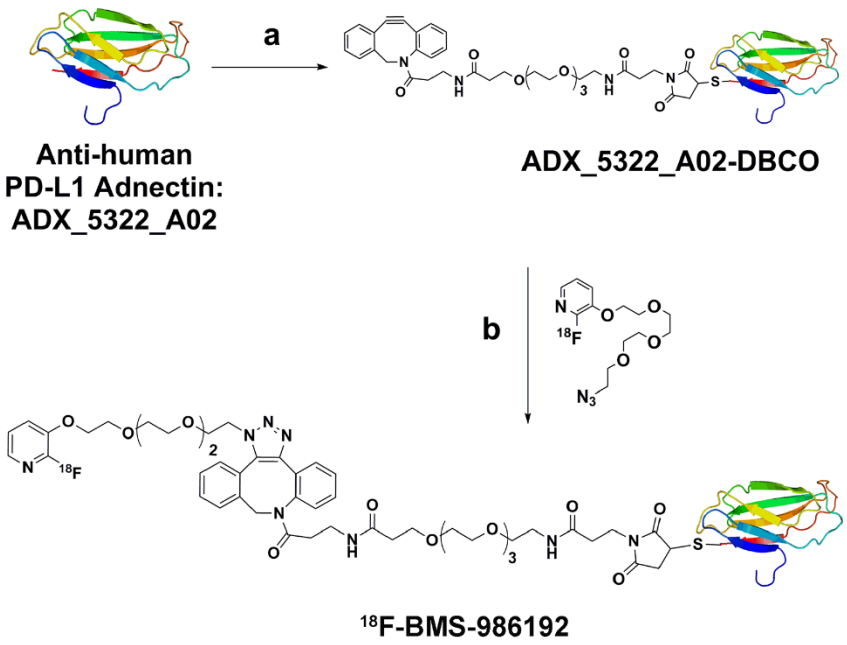

FIGURE 2. Synthesis of ^{18}F-BMS-986192. Reagents and Conditions: a) Maleimide-PEG4-DBCO 25 ^{o}C , 1 hr 1X PBS, pH 7.4/DMSO b) 1X PBS for 45 mins.

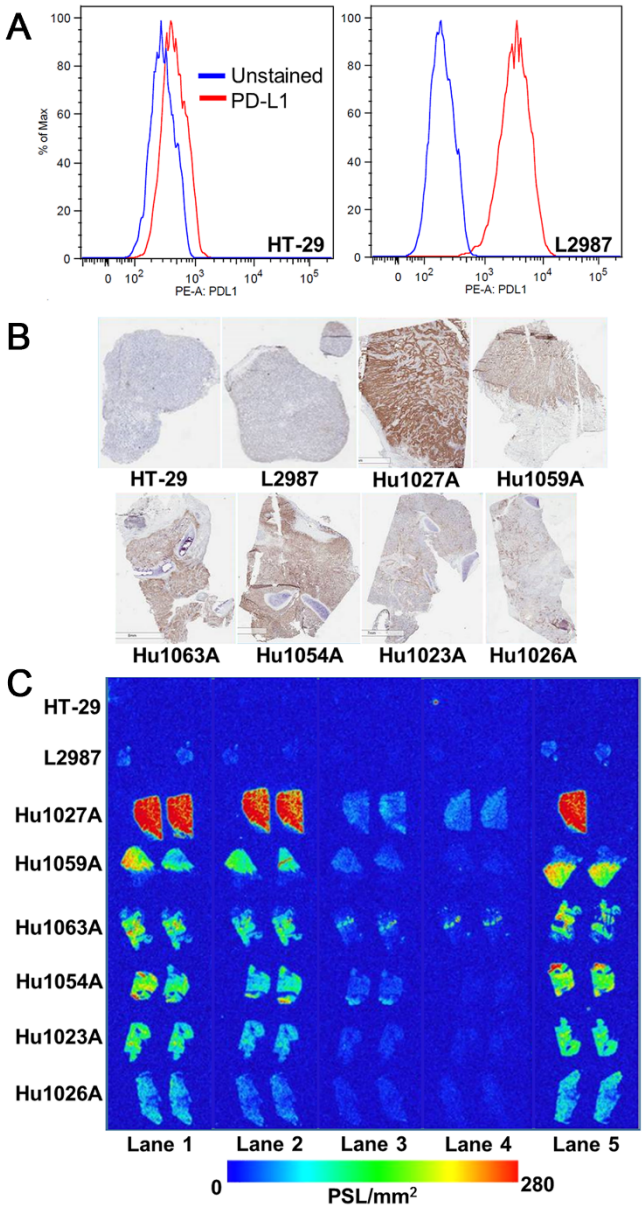

FIGURE 3. (A) Fluorescence-activated cell sorting analysis of HT-29 and L2987 cells. (B) Anti-PD-L1 immunohistochemistry staining of xenograft and human NSCLC tissues. (C) *In vitro* autoradiography of xenograft and human NSCLC tissue samples using ^{18}F-BMS-986192. Lane (1) Total binding of ^{18}F-BMS-

986192, Lane (2) 0.25 nM BMS-986192 blocking, Lane (3) 2.5 nM BMS-986192 blocking, Lane (4) 25 nM BMS-986192 blocking and Lane (5) 25 nM non-PD-L1 binding “sham” Adnectin control.

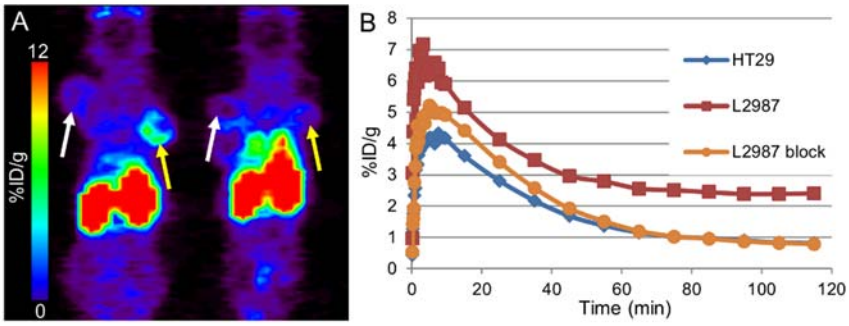

FIGURE 4. (A) Representative coronal PET images (slices) of two mice bearing bilateral PD-L1(+) L2987 (yellow arrows) and PD-L1(-) HT-29 (white arrows) tumors at 90-120 mins post ^{18}F-BMS-986192 administration. The left image shows tracer alone; the right image shows co-administration of 3 mg/kg BMS-986192. (B) Representative time-activity curves.

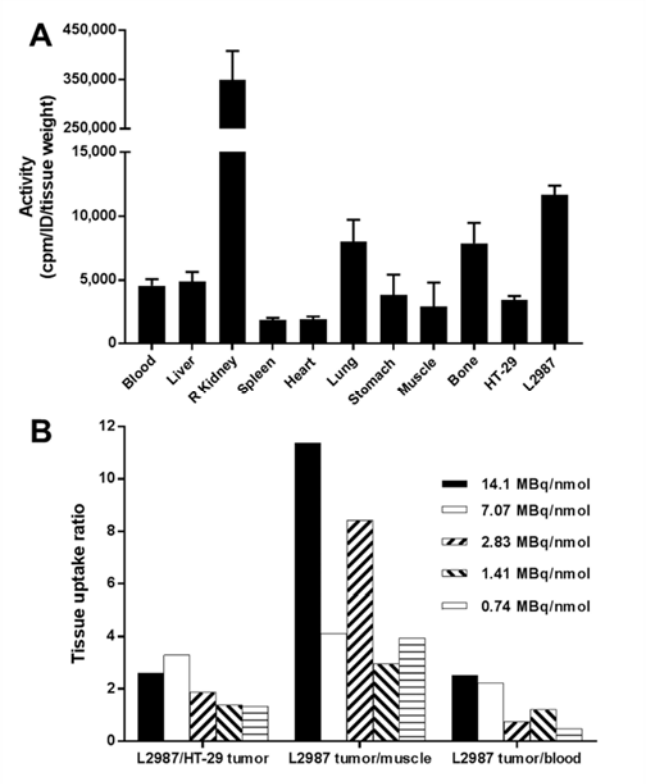

FIGURE 5. (A) *Ex vivo* biodistribution of ^{18}F-BMS-986192 in mice implanted with L2987 and HT-29 xenografts. Bars indicate mean ± SD (*n* = 4). (B) Contrast ratio of L2987 tumor uptake compared to control HT-29 tumors, skeletal muscle and blood.

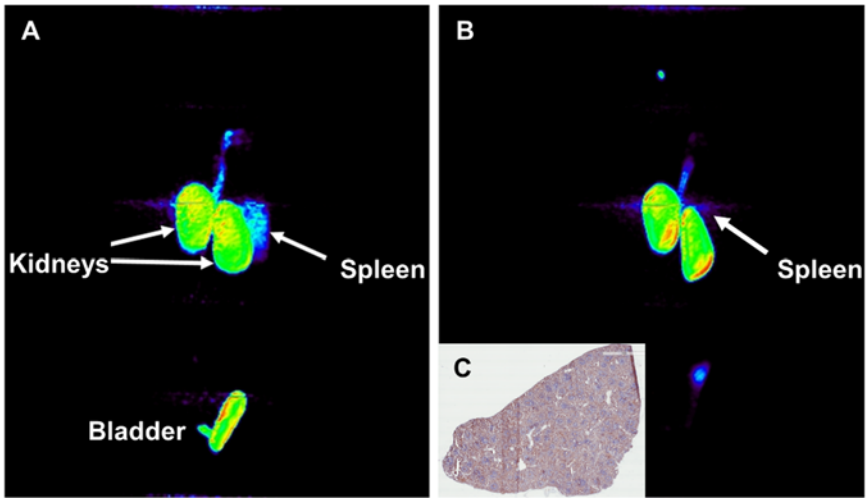

FIGURE 6. Representative whole-body PET (maximal intensity projection) images 90 mins post injection of (A) ^{18}F-BMS-986192 only (B) ^{18}F-BMS-986192 and co-administration of 1 mg/kg BMS-986192 in the same monkey. (C) Representative anti-PD-L1 immunohistochemistry of healthy monkey spleen tissue.

TABLE 1

^{18}F-BMS-986192 *In vitro* Autoradiography

Tissues	Total binding	+ BMS-986192 blocking				+ sham 25 nM
		0.025 nM	0.25 nM	2.5 nM	25 nM	
HT29	3.59	3.67	3.94	4.02	4.14	3.40
L2987	9.58	7.16	6.04	4.21	4.92	8.92
Hu1027A*	230.79	210.01	191.72	12.03	12.63	182.07
Hu1059A*	89.43	72.17	50.83	10.09	5.23	86.46
Hu1063A*	40.99	41.75	26.18	10.12	10.36	33.24
Hu1054A*	55.96	49.89	32.39	9.28	4.20	67.11
Hu1023A*	42.78	30.80	21.89	6.76	4.52	40.72
Hu1026A*	21.35	17.96	11.32	5.46	4.85	24.59

All values reported as mean PSL/mm^2.
*Denotes human NSCLC tumor sample.

SUPPLEMENTAL MATERIALS AND METHODS

General

^{18}F-Fluoride was purchased from P.E.T. Net Pharmaceuticals. Inc. or IBA Molecular. All reagents were obtained from Aldrich chemical company or Lancaster and were ACS grade or better except where noted.

Synthesis of ADX_5322_A02 Anti-PD-L1 Adnectin

Adnectins that bind specifically to human PD-L1 were selected from high-complexity libraries based on the 10th fibronectin type III domain using mRNA display, as described previously (*1–4*). The lead recombinant Adnectin, (Supplemental Table 1) was expressed in BL21(DE3) *E. coli* and purified from the soluble fraction using combinations of metal chelation, ion exchange, and gel filtration chromatography.

Synthesis of ADX_5322_A02-DBCO Anti-PD-L1 Adnectin

A 4-fold molar excess of maleimide-PEG4-DBCO was dissolved in DMSO and added to the purified modified ADX_5322_A02 anti-PD-L1 Adnectin in the presence of 1 mM tris(2-carboxyethyl)phosphine. Final DMSO concentrations did not exceed 5% in the conjugation mixtures. The reaction was monitored by mass spectroscopy and the sample was purified by size-exclusion chromatography using a HiLoad 26/60 Superdex 75 column equilibrated in phosphate buffered saline (PBS) at pH 7.2.

Synthesis of BMT-187144

A mixture of ((oxybis(ethane-2,1-diyl))bis(oxy))bis(ethane-2,1-diyl) bis(4-methylbenzenesulfonate) (5 g, 9.95 mmol) and sodium azide (0.647 g, 9.95 mmol) were dissolved in ethanol (50 mL) and the reaction was refluxed at 90 °C over a 17 hour period. The solvent was removed using partial vacuum and then loaded onto a 40 g silica cartridge. This compound was purified using flash chromatography (IscoCombiFlash - eluted using a linear gradient method starting from 10% ethyl acetate in hexanes going to a 90% ethyl acetate in hexanes over a 45 minute period). The pooled fractions were checked by tTLC and combined to give 2-(2-(2-(2-azidoethoxy)ethoxy)ethoxy)ethyl 4-methylbenzenesulfonate as a colorless oil. Due to the reactive nature of the 2-(2-(2-(2-azidoethoxy)ethoxy)ethoxy)ethyl 4-methylbenzenesulfonate product this material was used "as is" without any further characterization. To a suspension of sodium hydride (0.129 g, 3.21 mmol) in DMF (10 mL) at 0 °C was dropwise added a stirring solution of 2-fluoropyridin-3-ol (0.363 g, 3.21 mmol) in DMF (5 mL), then followed by the dropwise addition of the solution of 2-(2-(2-(2-azidoethoxy)ethoxy)ethoxy)ethyl 4-methylbenzenesulfonate (1.00 g, 2.68 mmol) in DMF (5 mL). The suspension was held at 0 °C for 10 minutes, then brought to ambient temperature for 1 hour, followed by additional heating at 60 °C for 4 hours. The solvent was removed in vacuo. 100 mL of ethyl acetate was added followed by 3 separate wash extractions with concentrated brine solution. The organic layer was dried over sodium sulfate, filtered, and concentrated. The crude material was purified using flash chromatography (IscoCombiFlash - eluted with 10-50% ethyl acetate in hexane) to give a colorless oil. 3-(2-(2-(2-(2-azidoethoxy)ethoxy)ethoxy)ethoxy)-2-fluoropyridine (BMT-187144) (702 mg, 2.233 mmol, 83% yield) was isolated as a clear oil. ^{1}H NMR (400 MHz, $CDCl_3$) δ 7.75 (dt, J =

4.9, 1.6 Hz, 1H), 7.33 (ddd, *J* = 10.0, 8.1, 1.5 Hz, 1H), 7.10 (ddd, *J* = 7.9, 4.9, 0.7 Hz, 1H), 4.30-4.16 (m, 2H), 3.95–3.83 (m, 2H), 3.80–3.61 (m, 10H), 3.38 (t, *J* = 5.1 Hz, 2H); ^{13}C NMR (100 MHz, $CDCl_3$) δ 142.3, 137.7, 137.5, 123.4, 123.4, 121.7, 121.6, 77.3, 76.7, 70.9, 70.7, 70.6, 70.0, 69.4, 69.0, 50.6; ^{19}F NMR (400 MHz, $CDCl_3$) δ -83.55; HRMS (ESI^+): *m/z* calcd for $[C_{13}H_{20}FN_4O_4]^+ = [M + H]^+$ 315.464, found 315.1463.

Synthesis of 3-(2-(2-(2-(2-azidoethoxy)ethoxy)ethoxy)ethoxy)-2-nitropyridine

Sodium hydride (0.121 g, 3.01 mmol) (60% suspension in oil) was dissolved in DMF (7.0 mL) and the resulting suspension was cooled to 0 °C. A solution of 2-nitropyridin-3-ol (0.384 g, 2.74 mmol) in DMF (1.5 mL) was added slowly, followed by the dropwise addition of 2-(2-(2-(2-azidoethoxy)ethoxy)ethoxy)ethyl 4-methylbenzenesulfonate (1.023 g, 2.74 mmol) in DMF (1.5 mL). The suspension was held at 0 °C for 10 minutes, then brought to ambient temperature for 2 hours followed by heating 60 °C for a 72 hour period. The reaction was quenched with 10 mL of DI water, followed by ethyl acetate extraction (3 x 10 mL). Pooled ethyl acetate extracts were washed with a concentrated brine solution (10 mL), dried over sodium sulfate, filtered, and evaporated under reduced pressure to give a light yellow oil. The crude was purified by flash chromatography. 24 g silica cartridge, 25 mL/min, starting from 10% ethyl acetate in hexanes, followed by a linear change to 50% ethyl acetate in hexanes over a 25 minute period. After this time, the gradient was held at this solvent composition for 10 minutes then changed to 100% ethyl acetate over a 10 minute period. 3-(2-(2-(2-(2-azidoethoxy)ethoxy)ethoxy)ethoxy)-2-nitropyridine was eluted between the 30-40 minute portion of the chromatogram and the pooled fractions were evaporated under reduced

pressure, then under vacuum for 2 hours to give 3-(2-(2-(2-(2-azidoethoxy)ethoxy)ethoxy)ethoxy)-2-nitropyridine (687 mg, 1.973 mmol, 72.0% yield) as a light yellow oil. ^{1}H NMR (400 MHz, $CDCl_3$) δ 8.11 (dt, J = 4.9, 1.6 Hz, 1H), 7.60 (ddd, J = 10.0, 8.1, 1.5 Hz, 1H), 7.52 (ddd, J = 7.9, 4.9, 0.7 Hz, 1H), 4.30–4.16 (m, 2H), 3.95–3.83 (m, 2H), 3.80–3.61 (m, 10H), 3.38 (t, J = 5.1 Hz, 2H); ^{13}C NMR (100 MHz, $CDCl_3$) δ 147.3, 139.5, 128.4, 124.4. 71.1, 70.7, 70.6,70.0, 69.9, 69.3, 50.7; HRMS (ESI^+): *m/z* calcd for $[C_{13}H_{20}N_5O_6]^+$ = [M + H] 342.1408, found 342.1409.

Surface Plasmon Resonance (SPR)

Binding properties of the anti-PD-L1 Adnectin and the non-radioactive reference Adnectin were compared by SPR using a Proteon XPR36 instrument (Bio-Rad). Biotinylated extracellular domains of human, cynomologus monkey, and mouse orthologs of PD-L1 recombinantly expressed and purified from HEK293 cells were captured on a neutravidin surface (NLC, BioRad) to a level of approximately 600 RU. Binding measurements were conducted at 25 °C in running buffer (PBS), pH 7.4, 0.05% Tween-20) by injecting a 5-point, 2-fold serial dilution series of each Adnectin analyte (concentrations ranging from 10 to 0.625 nM) and a blank over each PD-L1 ortholog surface at a flow rate of 50 µL/min for 120 seconds. Analyte injections were then stopped and dissociation was monitored for 800 seconds. To correct for non-specific analyte binding to the SPR chip, sensorgrams for each dilution series injection were double referenced by subtracting sensorgrams from blank injections and interspot NLC chip surfaces. Referenced data were then fitted using Proteon Manager software (Bio-Rad) to 1:1 Langmuir binding model to obtain k_a, k_d, and K_D values.

Cell Lines and Tumor Xenografts

The L2987 human lung carcinoma cell line was developed by BMS as previously described (*6*). HT-29 human colon adenocarcinoma carcinoma cells were obtained from the American Type Culture Collection. L2987 cells were cultured in Roswell Park Memorial Institute medium supplemented with 10% fetal bovine serum, while the HT-29 cells were cultured in Minimum Essential Media supplemented with 10% fetal bovine serum. All cells were maintained in a humidified incubator at 37 °C with 5% CO_2.

Fluorescence-activated Cell Sorting Analysis of Tumor Cell Lines for PD-L1 Expression

Fluorescence-activated cell sorting analysis of PD-L1 expression followed well described protocols. Briefly, HT-29 and L2987 human tumor cell lines were grown under culture conditions as described, harvested and resuspended in PBS + 0.5% BSA at 5×10^6 cells/mL. 200 μL (1×10^6 cells) was transferred into individual cell culture tubes, samples were pelleted at 200×g for 5 min, and the supernatant was aspirated. A staining buffer of R-PE conjugated anti-PD-L1 monoclonal antibody (eBioscience Cat# 12-5983-71) was prepared at a concentration of 5 μL/100 μL in PBS + 0.5% BSA. 100 μL staining buffer was added to each sample, cell pellets were pulse vortexed gently to mix, and samples were incubated on ice for 60 min. Following incubation, samples were washed with 2 mL PBS + 0.5% BSA and pelleted at 200×g for 5 min. Wash procedure was repeated for a total of

two washes, discarding supernatant between washes. Finally, cells were analyzed using an LSRII flow cytometer (Becton-Dickinson), gated to display live cells, and values displayed as relative R-PE fluorescence intensity.

Immunohistochemistry

Cryostat sections (5 μm) were fixed with acetone for 10 minutes at room temperature and stored at -80 °C until use. Anti-PDL1 antibody (clone 28-8) was used to stain tissue sections, with a commercial nonspecific Rabbit IgG (Abcam) used as an isotype control. PD-L1-expressing CHO-S cells and normal human placenta were used as positive controls. Immunostaining was performed using an indirect immunoperoxidase method at room temperature. Briefly, endogenous peroxidase activity was blocked by incubation for 10 minutes with a peroxidase block (Dako). To block non-specific binding, slides were incubated for 20 minutes with Dako protein block supplemented with 0.5% human gamma globulins for human tumor samples or with 0.1% mouse gamma globulins for mouse xenograft samples. Subsequently, primary antibodies (PD-L1-28-8 at 1, 3 or 5 μg/mL) or negative control (Rabbit IgG at 5 μg/mL) were applied to sections and incubated for 1 hour. Following washes with PBS, slides were incubated for 30 minutes with the peroxidase-conjugated anti-rabbit IgG polymer for human tumor samples or with peroxidase-conjugated anti-rabbit IgG polymer supplemented with 0.1% mouse gamma globulins for mouse xenograft tissues. Slides were then washed with PBS and reacted with the DAB substrate-chromogen solution for 6 minutes. Finally, slides were counterstained with

Mayer's hematoxylin and coverslipped with permount following routine histological procedure. Dako protein block was used as a diluent for all primary antibodies.

Radiation Dosimetry

A total of 4 cynomolgus monkeys (2 male, 3.5 kg each and 2 female, 3.3 and 3.4 kg) underwent whole body dynamic PET scanning on a Focus F220 scanner (Siemens) following i.v. injection of ^{18}F-BMS-986192 (47.8 ± 11.3 MBq). Subjects were scanned for ~6 hours in a sequence of 6 passes with 8 bed positions, covering each subject from top of head to lower leg. Scans were reconstructed using a filtered back projection algorithm with attenuation correction using the ^{57}Co transmission scans. Following image reconstruction, scans were visually inspected for organ activity concentrations exceeding background level. Source organs identified and utilized in the subsequent analysis were the kidneys, urinary bladder contents and heart. Regions of interest were drawn on these organs and mean activity values computed in order to form time activity curves of activity concentration (kBq/cm^3). Within-pass decay correction was removed to reflect actual activity in each organ, and cumulated activity (Bq*hr/cm^3) computed as integrals (by trapezoid rule) for data from the scan plus physical decay for the tail portion after the scan period. To correct for coarse scan timing at early time points, a value at t = 0 was added to each organ's time-activity curve before calculating the integrals as follows: 1) kidney - equal to first scan value; 2) myocardium - equal to twice the first scan value; 3) bladder - 0. Integrals were multiplied by the organ volumes of standard 70 kg adult male and 55 kg adult female reference mathematical phantoms (7), normalized by subject mass/70 kg and

then normalized to injected activity to obtain organ residence times. These values were entered into OLINDA 1.0 software to obtain absorbed doses in all organs.

Quality Control of ^{18}F-BMT-187144

Structural identity of the ^{18}F-BMT-187144 was confirmed by co-injection of the non-radioactive reference material 3-(2-(2-(2-(2-azidoethoxy)ethoxy)ethoxy)ethoxy)-2-fluoropyridine as shown in Supplemental Figure 1. Using an agilent 1100 analytical HPLC equipped with a posi-ram (LabLogic) radioactive detector in line with its flow path. A mixture of ^{18}F-BMT-187144 and 3-(2-(2-(2-(2-azidoethoxy)ethoxy)ethoxy)ethoxy)-2-fluoropyridine were loaded into a Luna (Phenomenex) C-18(2) 3 micron column (4.6 x 150 mm) with a gradient program using a mobile phase that went from 10% acetonitrile in aqueous 0.1% trifluoroacetic acid (TFA) at a flow rate of 1 mL/min to 90% acetonitrile in aqueous 0.1% TFA at a flow rate of 1 mL/min over 18 minutes. UV detector was set at 280 nm and these peaks co-eluted within 0.1 minutes.

Quality Control of ^{18}F-BMS-98619

Structural identity of the ^{18}F-BMS-986192 was confirmed by co-injection of the non-radioactive reference material ADX_5322_A02 and gel filtration reference standard (Bio-Rad, 1610375) containing a mixture of five proteins ranging from 1,350 – 670,000 Da, as shown in Supplemental Figures 2 and 3. Using an Agilent 1100 analytical HPLC equipped with a posi-ram (LabLogic) radioactive detector in line with its flow path. A mixture of ^{18}F-BMS-986192 and ADX_5322_A02 Adnectins or and Bio-Rad gel filtration reference standard were loaded onto a Superdex 200 10/300 GL size exclusion chromatography column using an isocratic HPLC program using a mobile phase of 100%

1X PBS buffer at pH 7.4 at a flow rate of 0.5 mL/min UV detector was set at 280 nm. Co-injection with Bio-Rad gel filtration reference standard confirmed the ^{18}F-BMS-986192 Adnectin eluted with a protein consistent with 11-12 kDa size and co-eluted with 0.1 minutes of the ADX_5322_A02 reference standard using this method (Supplemental Fig. 3).

Determination of Specific Activity

The specific activity of ^{18}F-BMS-986192 was measured using a nano-drop 2000 UV-Vis Spectrophotometer (Thermo). A brief example of this process, 0.5-2 μL samples consisting of ^{18}F-BMS-986192 was placed on the nano-drop 2000 and the protein concentration of these samples was measured against an internal reference standard at 280 nm. These samples were run in triplicate and the specific activities were calculated as a function of the total isolated radioactivity of the purified sample. 1.0 GBq of ^{18}F-BMS-986192 was isolated in a 2 mL total volume and the protein concentration of this sample was 0.095 mg/mL, giving a 0.195 mg total protein concentration and a calculated specific activity of 62.5 MBq/nmol.

Stability of ^{18}F-BMT-187144 in 1X PBS

100 μL solution of 0.74 GBq ^{18}F-BMT-187144 was stirred at 23 °C for 1 hour in a solution containing 200 μL of 1X PBS to mimic the coupling conditions for complex biologic molecules. After this time this samples was analyzed using a Varian Prostar analytical HPLC equipped with a gamma ram (LabLogic) radioactive detector in line with its flow path. A 10 μL sample of a mixture of ^{18}F-BMT-187144 and 3-(2-(2-(2-(2-

azidoethoxy)ethoxy)ethoxy)ethoxy)-2-fluoropyridine was loaded into a Luna (Phenomenex) C-18(2) 3 micron column (4.6 x 150 mm) with a gradient program using a mobile phase that went from 10% acetonitrile in aqueous 0.1% trifluoroacetic acid at a flow rate of 1 mL/min to 90% acetonitrile in aqueous 0.1% TFA at a flow rate of 1 mL/min over 25 minutes. UV detector was set at 280 nm and these peaks co-eluted with 0.1 minutes using this method. >70% ^{18}F-BMT-187144 remained intact after this study (Supplemental Fig. 7).

^{18}F-BMT-187144 Concentration (Volatilization) Study

To show the prosthetic group, ^{18}F-BMT-187144 could be concentrated from ethanol and reconstituted into 1X PBS buffer without loss of radioactivity, a volatilization study was conducted in the following manner. 1.4-14.8GBq, ^{18}F-BMT-187144 in 1,000-3,000 μL of ethanol was concentrated, using a 70 °C oil bath, vacuum and a gentle stream of nitrogen gas. The ethanol volume was reduced to varying concentrations between 100-5 μL and the sample was removed and measured in the dose calibrator and decay corrected. Between 90-98% of the radioactivity remained when ethanol was reduced from 3,000 μL to <5 μL in this study.

Radiometabolite Analysis in Rodent Plasma

RadioTLC was completed on a Bioscan AR2000 using uniplate – Silica Gel GHLF, scored 10 x 20 cm, 250 microns TLC plates and an 8% methanol in dichloromethane as the solvent. 6.4-7.4 MBq of ^{18}F-BMS-986192 was injected into Athymic BALB/C mice (Harlan) and these animals were maintained on 1-2% isoflurane

during injection, tracer uptake, and blood sampling. 100 μL aliquots samples of blood were collected in lithium heparin coated tubes either from the contralateral tail vein or the retro-orbital plexus at 15, 60 and 100 minutes after ^{18}F-BMS-986192 injection. These samples were centrifuged for 10 minutes at 10,000 rpm and 4 °C for plasma separation and washed with equal amounts of methanol. 10 μL of the methanol extract of plasma was co-spotted with non-radioactive reference compound onto and across the TLC plates (Silica Gel GHLF; Scored 2.5 x 10 cm; 250 microns), blow-dried with warm air and developed in a TLC chamber. The TLC solution used in this study was is 8% methanol in dichloromethane which gave an R_f ~ 0.4. After the development was completed, the TLC plate was placed onto the radio-TLC scanner (Bioscan, AR2000), which scanned the TLC plate for 15 minutes. The peak areas were calculated to give the metabolite profile of ^{18}F-BMS-986192 which shows this PET radioligand was 100% intact over the course of this study as shown in Supplemental Figure 6.

Pharmacokinetics

Male cynomolgus monkeys (n = 3) were intravenously administered a single dose of BMS-986192 (1 mg/kg). Serum samples were collected at 1, 2, 4, 7, and 24 hours post dose. Urine samples were collected at intervals of 0-7 hours and 7-24 hours. Serum concentrations of BMS-986192 were determined by a ligand binding assay. This assay method used two mouse monoclonal antibodies for the capture and detection of analytes. Both monoclonal antibodies bind specifically to the Adnectin scaffold but with different binding epitopes. In addition to the LBA, a liquid chromatography-high resolution mass spectrometry method was also used to verify the identity of analytes in monkey serum and

urine, and to quantify compounds in urine samples. In general, BMS-986192 and ADX_5322_A02-DBCO had very similar serum pharmacokinetic profiles. Compounds were eliminated rapidly from monkeys with T-HALF of 1.4-1.7 h. Clearance values of BMS-986192 and ADX_5322_A02-DBCO were 4.54 and 5.78 mL/min/kg, respectively. The volume of distribution at steady state (Vss) was low for both compounds, ranging from 0.2 to 0.4 L/kg. Supplemental Figure 7 shows the serum concentration versus time curves of each compound ($n = 3$). Urinary recovery of both compounds was variable, ranging from <0.5% to 11.3% of dose in the case of ADX_5322_A02-DBCO. Mean urinary excretion was comparable between the two compounds, with 5.8% and 6.5% total dose excreted in the urine for BMS-986192 and ADX_5322_A02-DBCO respectively.

SUPPLEMENTAL FIGURES

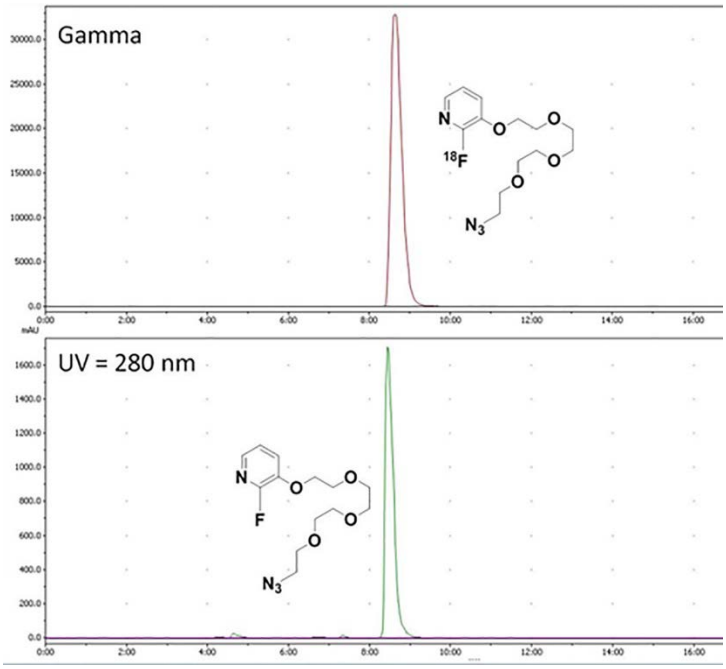

SUPPLEMENTAL FIGURE 1. Analytical HPLC of ^{18}F-BMT-187144 co-injected with non-radioactive reference standard using a reverse phase HPLC method.

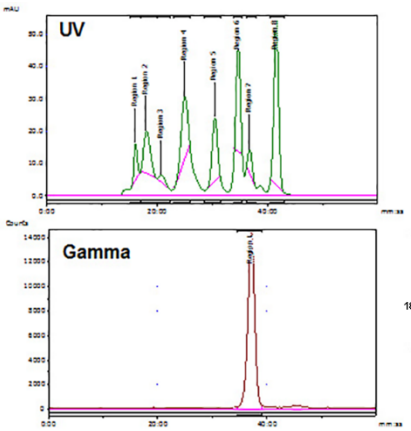

Name	Retention (mm:ss)
670 kDa	17:57
158 kDa	24:55
44 kDa	30:22
17 kDa	34:36
11 kDa	36:39
1.35 kDa	41:29

Name	Retention (mm:ss)	%ROI (%)
^{18}F-BMS-986192	37:02	100.00
1 Peak		100.00

SUPPLEMENTAL FIGURE 2. HPLC chromatogram ^{18}F-BMS-986192 anti-human -PD-L1 Adnectin co-eluted with non-radioactive Bio-Rad gel filtration reference standard reference standard using Superdex 200 10/300 GL size exclusion column.

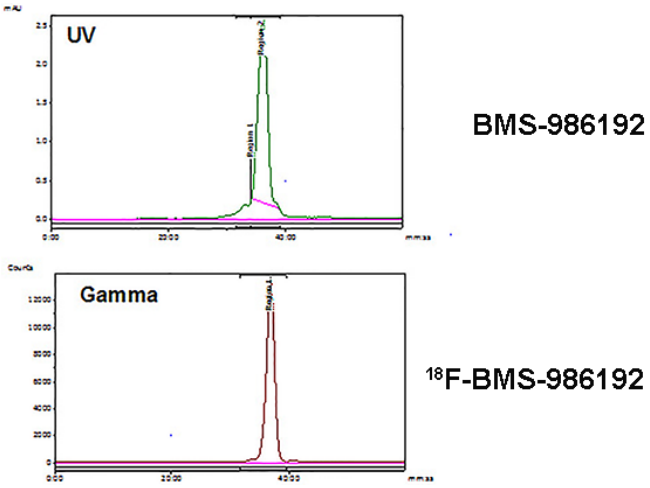

SUPPLEMENTAL FIGURE 3. HPLC chromatogram ^{18}F-BMS-986192 anti-human PD-L1 Adnectin co-eluted with non-radioactive ADX_5322_A02 reference standard reference standard using Superdex 200 10/300 GL size exclusion column.

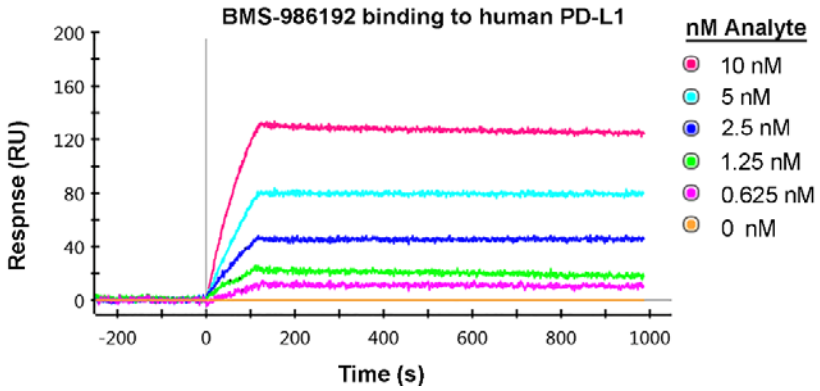

SUPPLEMENTAL FIGURE 4. SPR data to determine binding to human PD-L1 using BMS-986192.

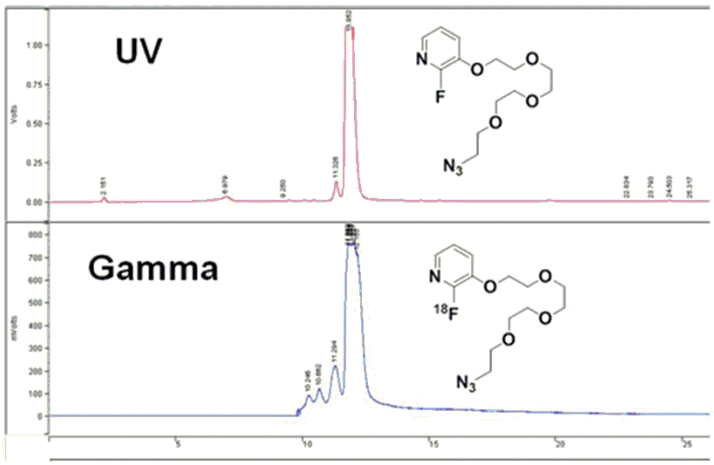

SUPPLEMENTAL FIGURE 5. Analytical HPLC of ^{18}F-BMT-187144 co-injected with non-radioactive reference standard using a reverse phase HPLC method showing the 1 hour stability time point of ^{18}F-BMT-187144 in 1XPBS buffer at 23 °C

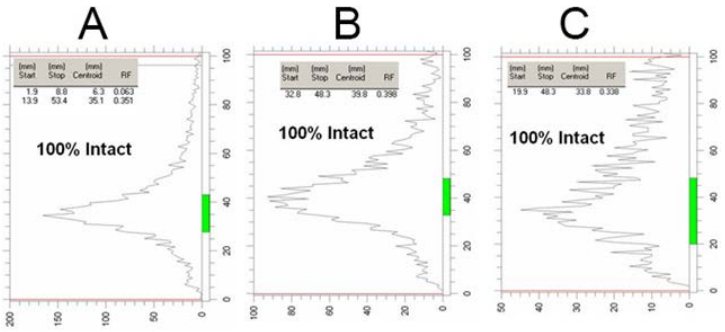

SUPPLEMENTAL FIGURE 6. *In vivo* plasma radiometabolite analysis of ^{18}F-BMS-986192. RadioTLC analysis of plasma extracts of ^{18}F-BMT-986192 A) 15 minutes; B) 60 minutes; C) 100 minutes post-injection in Athymic BALB/C mice

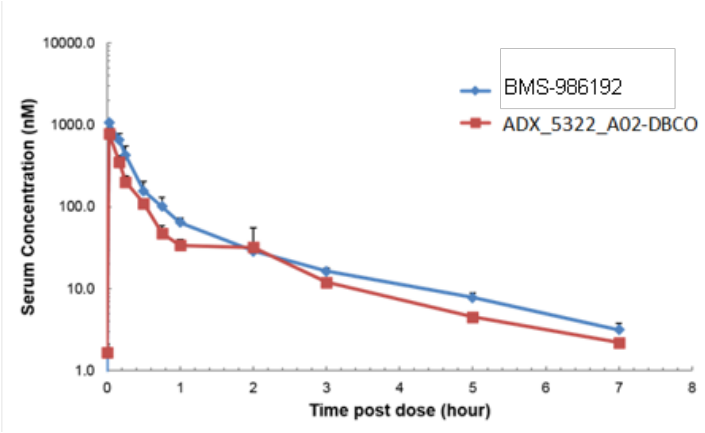

SUPPLEMENTAL FIGURE 7. Concentration versus time profile of BMS-986192 and ADX_5322_A02-DBCO in cynomolgus monkey serum. Both molecules demonstrated rapid clearance from the serum (T-HALF 1.4 - 1.7 h)

SUPPLEMENTAL TABLES

SUPPLEMENTAL TABLE 1. Sequence Information for ADX_5322_A02 Anti-human PD-L1 Adnectin

DESCRIPTION	SEQUENCE
ADX_5322_A02	MGVSDVPRDLEVVAATPTSLLISWSYDGPIDRYY
anti-human PD-L1	RITYGETGGNSPVQEFTVPPDQKTATISGLKPGV
Adnectin	DYTITVYAVRLEEAHYNREFPISINYRTPC

SUPPLEMENTAL TABLE 2. Adnectin Binding to Immobilized PD-L1 Orthologs by Surface Plasmon Resonance

Construct	PD-L1 Ortholog Attached to Surface	k_a ($M^{-1}s^{-1}$)	k_d (s^{-1})	K_D (pM)
ADX_5322_A02	Human PD-L1	$>1x10^6$	$<1x10^{-5}$	<10 pM
ADX_5322_A02	Cynomolgus PD-L1	$>1x10^6$	$<1x10^{-5}$	<10 pM
^{19}F-BMS-986192	Human PD-L1	$>1x10^6$	$<1x10^{-5}$	<10 pM
^{19}F-BMS-986192	Cynomolgus PD-L1	$>1x10^6$	$<1x10^{-5}$	<10 pM

*No binding observed using murine PD-L1 with all of the Adnectins tested.

SUPPLEMENTAL TABLE 3. ^{18}F-BMS-986192 Cynomolgus Dosimetry (mSv/MBq)

Organ	Male		Female		Average
	B4325	B4345	B2153	B5045	
Adrenals	5.41E-03	5.78E-03	1.09E-02	9.59E-03	7.92E-03
Brain	5.14E-06	9.27E-06	1.573-05	1.43E-05	1.11E-05
Breasts	2.21E-04	3.81E-04	5.32E-04	4.86E-04	4.05E-04
Gallbladder Wall	3.03E-03	3.24E-03	5.00E-03	4.22E-03	3.87E-03
LLI Wall	1.96E-03	2.32E-03	4.73E-03	2.02E-03	2.76E-03
Small Intestine	2.12E-03	2.32E-03	4.62E-03	3.19E-03	3.06E-03
Stomach Wall	1.86E-03	2.05E-03	3.14E-03	2.70E-03	2.44E-03
ULI Wall	1.94E-03	2.12E-03	3.97E-03	2.84E-03	2.72E-03
Heart Wall	6.14E-04	5.59E-03	4.54E-03	5.05E-03	3.95E-03
Kidneys	1.73E-01	1.81E-01	2.78E-01	2.47E-01	2.20E-01
Liver	2.16E-03	2.38E-03	3.97E-03	3.46E-03	2.99E-03
Lungs	5.27E-04	8.00E-04	1.34E-03	1.22E-03	9.72E-04
Muscle	1.14E-03	1.31E-03	2.37E-03	1.60E-03	1.60E-03
Ovaries	N/A	N/A	4.92E-03	2.30E-03	3.61E-03
Pancreas	3.78E-03	4.11E-03	6.59E-03	5.78E-03	5.07E-03
Red Marrow	1.62E-03	1.81E-03	3.11E-03	2.38E-03	2.23E-03
Osteogenic Cells	7.78E-04	8.84E-04	1.70E-03	1.31E-03	1.17E-03
Skin	5.08E-04	5.78E-04	9.78E-04	6.95E-04	6.90E-04
Spleen	4.92E-03	5.19E-03	9.05E-03	7.92E-03	6.77E-03
Testes	1.08E-03	1.31E-03	N/A	N/A	1.19E-03
Thymus	2.02E-04	6.84E-04	6.68E-04	6.73E-04	5.57E-04
Thyroid	6.19E-05	9.32E-05	1.07E-04	9.89E-05	9.03E-05

Urinary Bladder Wall	5.30E-02	6.46E-02	1.49E-01	5.00E-02	7.91E-02
Uterus	N/A	N/A	8.62E-03	3.41E-03	6.01E-03
Total Body	1.81E-03	2.02E-03	3.68E-03	2.78E-03	2.57E-03
Effective Dose	8.27E-03	9.27E-03	1.72E-02	1.04E-02	1.13E-02

SUPPLEMENTAL TABLE 4.
^{18}F-BMT-187144 Concentration Study

^{18}F-BMT-187144 isolated (GBq)	Starting volume ethanol (µL)	Ending volume of ethanol (µL)	^{18}F-BMT-187144 remaining (GBq)	% retained after concentration
1.85	1000	100	1.78	96%
1.86	1000	50	1.82	98%
1.90	1000	10	1.75	92%
1.70	1000	<5	1.53	90%
14.8	3000	<5	14.1	90%

SUPPLEMENTAL REFERENCES

1. Koide S, Koide A, Lipovsek D. Target-binding proteins based on the 10th human fibronectin type III domain ((1)(0)Fn3). *Methods Enzymol.* 2012;503:135-156.

2. Xu L, Aha P, Gu K, et al. Directed evolution of high-affinity antibody mimics using mRNA display. *Chem Biol.* 2002;9:933-942.

3. Kurz M, Gu K, Lohse PA. Psoralen photo-crosslinked mRNA–puromycin conjugates: a novel template for the rapid and facile preparation of mRNA–protein fusions. *Nucleic Acids Research.* 2000;28:e83-e83.

4. Roberts RW, Szostak JW. RNA-peptide fusions for the in vitro selection of peptides and proteins. *Proc Natl Acad Sci U S A.* 1997;94:12297-12302.

5. Lipovsek D. Adnectins: engineered target-binding protein therapeutics. *Protein Eng Des Sel.* 2011;24:3-9.

6. Friedman PN, Chace DF, Trail PA, Siegall CB. Antitumor activity of the single-chain immunotoxin BR96 sFv-PE40 against established breast and lung tumor xenografts. *J Immunol.* 1993;150:3054-3061.

7. Stabin MG, Sparks RB, Crowe E. OLINDA/EXM: the second-generation personal computer software for internal dose assessment in nuclear medicine. J Nucl Med 2005; 46: 1023-1027.